EVALUATING THE STRUCTURAL, MORPHOLOGICAL AND OPTICAL PROPERTIES OF PURE AND COBALT DOPED BISMUTH VANADATE NANOPOWDER BY CHEMICAL PRECIPITATION METHOD

N. KARTHI[a], K. A. RAMESHKUMAR[b*], P. MAADESWARAN[c]
[a]*Department of Energy Studies, Periyar university, Salem – 636 011, Tamilnadu, India*
[b]*Department of Energy Studies, Periyar university, Salem – 636 011, Tamilnadu, India*
[c]*Department of Energy Studies, Periyar university, Salem – 636 011, Tamilnadu, India*

Pure $BiVO_4$, Cobalt doped $BiVO_4$ nanoparticles prepared by Co-precipitation method and assessed for their structural, morphological and optical properties. The synthesized Pure $BiVO_4$ and Co-$BiVO_4$ nanoparticles were characterized by using XRD,FTIR, UV-DRS, SEM,EDS and Photoluminescence spectra (PL). XRD pattern shows the purity of prepared Pure $BiVO_4$ and Co-$BiVO_4$ nanoparticles size range of 5.6-22.3 nm and exhibit orthorhombic crystalline phase. Scanning Electron Microscopy (SEM) shows some clusters with tiny particles which revealed remarkable change in morphology of the prepared samples. The functional groups confirmation and chemical bonding confirmation was performed by FTIR and UV-DRS analysis. The estimated optical band gap to be 2.842 eV- 2.538 eV. The imperfection conditions were exposed from the Ultraviolet and visible emissions of the PL spectra.

(Received October 2, 2020; Accepted January 22, 2021)

Keywords: $BiVO_4$, Cobalt doped $BiVO_4$, Co-precipitation, UV-DRS

1. Introduction

Nano materials have little mass and are dominated by surface area to volume ratio and size effects, the processes and equipment for nanotechnology based manufacturing are expected to differ significantly from those currently used. In medical and biomedical sciences nanomaterials are used in diagnosis, therapeutic applications, surgery and artificial implants, drug delivery, hyperthermia, advanced imaging, medical rapid tests, prostheses and implants, antimicrobial agents and coatings agents in cancer therapy [1, 2]. Is the inorganic compound with the formula $BiVO_4$, It is a bright yellow solid. It is widely used as visible light photo-catalyst with a narrow band gap of less than 2.4 eV. More specifically Bismuth Vanadate is a mixed-metal oxide with the advantage of a very simple and cheap material and it has been considered as one of the important visible light driven photo catalysts [3, 4]. Basically $BiVO_4$ based compounds are extensively studied as the potential substitutes for the lead, cadmium and chromate-based pigments that are widely used in the coating and plastics industry, because of their non-toxic nature with wide band gap of 2.4 eV [5, 6] .The doping of various transition metal cations (V, Cr, Mn, Fe, Co and Ni) and anions (N, S, C or B) into semiconductors are used to improve the photo-activity under visible-light irradiation. The metal doping is a way to improve the utilization of solar light for semiconductors by modifying the band gap structures. A small amount of impurities added into the material may also change the electrical, optical and surface properties. The doping concentration of the metal with $BiVO_4$ and calcination process induces some changes in the structure, physical and chemical properties of prepared nanomaterials ($BiVO_4$) [7, 8]. Among the dopants, Co is one of the most favorable metal for amalgamate with $BiVO_4$, since its valence; ionic radii are closer to that of Bi^{3+}. So Bi^{3+} replaced by Co^{2+} which gives high donor effect, charge separation and transport in the $BiVO_4$ nanostructure. Bismuth Vanadate can be more useful when used as

* Corresponding author: nkarthiphysics1985@gmail.com

photo anode, which has the ability of water oxidation to O_2 in half reaction and CO_2 to other bio-products/bio-fuels. Monoclinic form of Bismuth Vanadate has found to be the most photo-catalytically active. Some merits of metal doped $BiVO_4$ are (i) High photon absorbance performance due to its narrow band gap of 2.4 eV, (ii) Its thermodynamic level is close to hydrogen, with its VB position negative enough with respect to water, (iii) Improved extraction and separation of electron-hole pairs as the estimated effective masses for holes and electrons is lower than similar semiconductors (eg: TiO_2 or In_2O_3) and (iv) Bismuth Vanadate has non-toxic properties, so this material is preferred as photo anode material. $BiVO_4$ and metal doped $BiVO_4$ nanoparticles are prepared by various methods such as RF Sputtering, Thermal Evaporation, Wet Chemical, Reflux, Hydro Thermal, Solvo-thermal, Hydrothermal, Sol gel, and Spin coating techniques have also been reported by many researchers [9, 10]. In this present work pure $BiVO_4$ and various concentration (3, 5 and 7%) of Cobalt doped $BiVO_4$ nanoparticles have been prepared by chemical co- precipitation method and the prepared samples are characterized through various techniques like X-RD, SEM-EDS,PL and UV study etc. and the results of their structural, morphological and optical properties have been discussed.

2. Experimental details

2.1. Materials

Bismuth Nitrate (Bi $(NO_3)_3$-$5H_2O$ - Sigma Aldrich 98%), Ammonium meta Vanadate (NH_4VO_3-HIMEDIA 98-102%), Cobalt Nitrate ($CO(NH_2)_2$), PVP (HIMEDIA), Sodium Hydroxide pellets, Ethanol and deionised water.

2.2. Methods

The analytical grade (AR), Ammonium Meta Vanadate (NH_4VO_3), Bismuth Nitrate (Bi $(NO_3)_3$-$5H_2O$) and Cobalt Nitrate (CO $(NH_2)_2$) were used as starting materials. The typical synthesis process is as follows: the stoichiometric amount of 1.40376 g Ammonium Meta Vanadate and 2.91042 g of Bismuth Nitrate were dissolved in 20 ml of deionized (DI) water separately under stirring. Still, the pH of the obtained aqueous solution was adjusted to approximately 9.0 by adding the concentrated HCl. The precursor solutions were rapidly mixed together to form a homogeneous mixture. After that, a required 0.15 g of PVP was added drop wise to the above mixture over 20 minutes at room temperature. Finally, a requisite amount of NaOH was added to the above precursor solution under constant stirring at 60^{o}C for 24 h. Then, the reactants were introduced in this order and stirred for a few minutes until the solution turned to yellow colour. Later on, the obtained yellow colour precipitate was collected and washed with acetone, ethanol and deionized water (20 ml). In addition, the precipitate is dried for 4 h at 60°C and it was slightly grounded. Finally, the above products were heated in a muffle furnace with 5^{o}C/min heating rate at 450^{o}C for 2 h and cooled to room temperature. Similarly, the Co doped $BiVO_4$ with different dopant concentration (3, 5 and 7%) were also synthesized using the same procedure using doping source materials.

2.3. Characterization techniques

The Prepared samples studied using various techniques shown in following Table 1.

Table 1. Characterization studies for Synthesized Nanoparticles.

Purpose	Characterization studies	Conditions
Size and Shape	X-ray Powder Diffraction - XRD	Philips Analytical Model Bruker D8 Advance Twin-Twin.
Structure and Surface morphology	HR-field emission Scanning Electron Microscope- HRSEM	JEOL 6390LA - Accelerating voltage: 0.5 to 30 kV, Filament: Tungsten.
Elemental composition analysis	Energy-Dispersive X-ray Spectrometer-EDS	OXFORD XMXN-EDAX resolution-136eV, EDAX detector area: 30 mm^2.
Absorption studies	UV-Vis Diffuse Reflectance Spectral -UVDRS	Recorded from 200 to 1400 nm.
Optical studies	Photoluminescence (PL)	Spectrum recorded from 450 to 700 nm

3. Result and discussion

3.1. XRD Structural analysis

Fig. 1 shows the powder X-ray diffractograms (XRD) of Co doped $BiVO_4$ and pure $BiVO_4$ nanoparticles synthesized by co-precipitation method. The XRD of pure $BiVO_4$ is in complete agreement with JCPDS card no.74-1717 revealing the orthorhombic crystalline phase with lattice parameters a=5.332, b=5.06 and c=12.02. The peaks correspond to the orthorhombic structure of $BiVO_4$ showing preferred orientations along (013), (200), (024) and (311) planes.

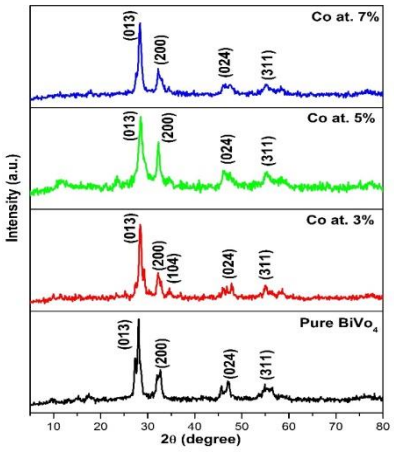

Fig. 1. XRD of synthesized Pure $BiVO_4$ and Various concentration of Co doped $BiVO_4$ NPs.

The observed pattern of Co doped $BiVO_4$ samples reveal that there is no impurity phase but there is a small shift in the 2θ value of the diffraction peaks to higher angle when compared to pure $BiVO_4$ diffraction pattern [11]. Crystalline sizes of $BiVO_4$ and Co doped $BiVO_4$ were calculated using below debye-scherrer's equation (1).

$$D = k\lambda / \beta \cos\theta \quad (1)$$

where D is the crystallite size, k is the Scherrer constant is usually taken as 0.89, λ is the wavelength of the X-ray radiation (CuKα= 0.1542 nm), β is the peak full width at half-maximum (FWHM) and θ is the diffraction peak angle. The average size of the crystalline domains in Co doped $BiVO_4$ is situated in the range of 5.6-22.3 nm with the lowest size in the lightly doped sample. The values of 2θ, Miller indices and full-width half maximum and calculated crystallite size were tabulated in Table 2. The dislocation density 'S' is a measurement of amount of defects and vacancies in the crystal which can be determined from the particle size "D" using the below equation (2).

$$S = 1/D_2 \quad (2)$$

It can be seen from the Table 1 that S decreasing from 0.020 × 1014 to 0.006 × 1014 with increasing Co content. It indicates that the lattice imperfection increases with particle size. Micro-strain can be calculated using the equation (3).

$$Micro - strain = \beta \cos\theta /4 \quad (3)$$

It has been observed that the micro-strain varies between 0.119×10^4 and 0.156×10^4 as the Cobalt content is increased from 3% to 7%. In general, variation in micro-strain may be due to the transformation in morphology, crystallite size and shape of the particles. The atoms trapped in the non-equilibrium position could shift to equilibrium position and it could release the strain [12]. The observed increase in micro-strain is attributed to the increase in crystal size.

Table 2. Structural parameters of pure and Co doped $BiVO_4$ samples at 450^{o}C for 2 h.

$BiVO_4$	**2θ (degree)**	**d-spacing**		**FWHM (degree)**	**Crystallite size (D) nm**	**Dislocation density (10^{14} lines/m^2)**	**Micro-strain (ε) 10^4lin^{-2}m^{-4}**
		hkl	**(nm)**				
0%	28.0367	13	3.18	0.587	13.9558	0.005134	0.159064
	32.6	200	2.74454	0.6778	12.2172	0.0067	0.159642
	45.6576	24	1.98542	0.5724	15.0648	0.004406	0.176362
	54.8	311	1.67384	0.75	11.9354	0.00702	0.174838
3%	28.5116	13	3.1281	1.1767	6.9691	0.020589	0.119266
	32.2542	200	2.77317	0.9449	8.756	0.013043	0.143062
	46.2	24	1.96336	1.0888	7.9357	0.015879	0.155541
	55.3708	311	1.65793	1.5917	5.6385	0.031454	0.147142
5%	28.3278	13	3.14798	0.7475	10.9662	0.008315	0.148403
	32.3	200	2.76934	0.78	10.6084	0.008886	0.153086
	46	24	1.97143	0.6888	12.5348	0.006364	0.171773
	55.1666	311	1.66358	1.1333	7.9118	0.015975	0.162228
7%	28.407	13	3.13938	0.6353	12.9052	0.006004	0.15629
	32.9	200	2.72019	0.3714	22.3134	0.002008	0.178144
	46.8173	24	1.9389	0.5082	17.0413	0.003443	0.179606
	54.9964	311	1.66832	0.8237	10.8772	0.008452	0.172473

3.2. SEM analysis

Fig. 2 shows the scanning electron microscope images of the pure $BiVO_4$ and Co doped $BiVO_4$ nanoparticles. Morphology of prepared samples was investigated by SEM. The Cobalt doping has an obvious effect on the morphology of the $BiVO_4$ nanoparticles. It is important to note that the morphology of doped sample Fig. 2 (b), (c), (d) shows some clusters with tiny particles

appear, which are maintaining same as observed in undoped $BiVO_4$, when Co was doped into $BiVO_4$ lattice and the result is in good agreement. The particles tend to agglomerate with one another due to increase in surface area to volume ratio which results an increase in attractive force between the nanoparticles. This growth was attributed to the successfully doped Co into a $BiVO_4$ lattice. The SEM micrographs also reveal that Co doping in $BiVO_4$ nanoparticles can increase the average crystallite size, this result agrees with our XRD measurements.

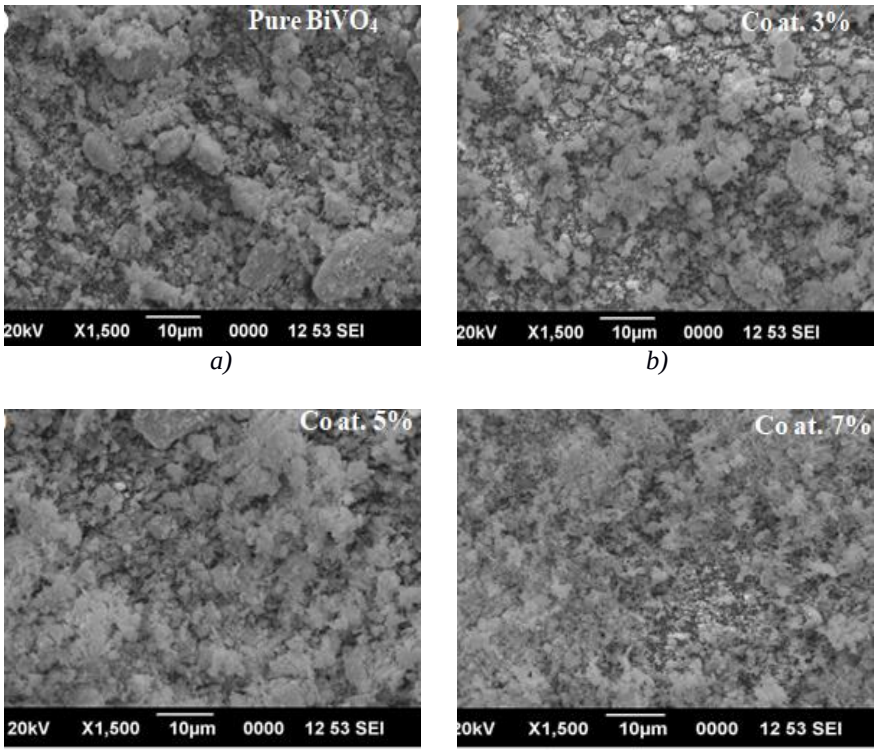

Fig. 2. SEM image of synthesized a) Pure $BiVO_4$ b) 3% Co doped $BiVO_4$ c) 5% Co doped $BiVO_4$ & d) 7% Co doped $BiVO_4$ nanoparticles.

3.3. EDAX Analysis

Fig. 3 presents the energy dispersive X-ray (EDX) spectra of the synthesized Cobalt doped and undoped $BiVO_4$ nanoparticles. The EDX spectrum of pure $BiVO_4$ shows the presence of Bismuth, Vanadium and Oxygen. The absence of any other element reveals the purity of the prepared sample. The EDX spectra of the doped $BiVO_4$ confirm doping $BiVO_4$ with cobalt. Furthermore, the absence of any element other than Bismuth, Vanadium, Cobalt and Oxygen shows the purity of the synthesized doped nanoparticles. The atomic percentages of Cobalt doping, determined by EDX analysis, in the synthesized doped materials are 2.46, 3.63 and 6.26.

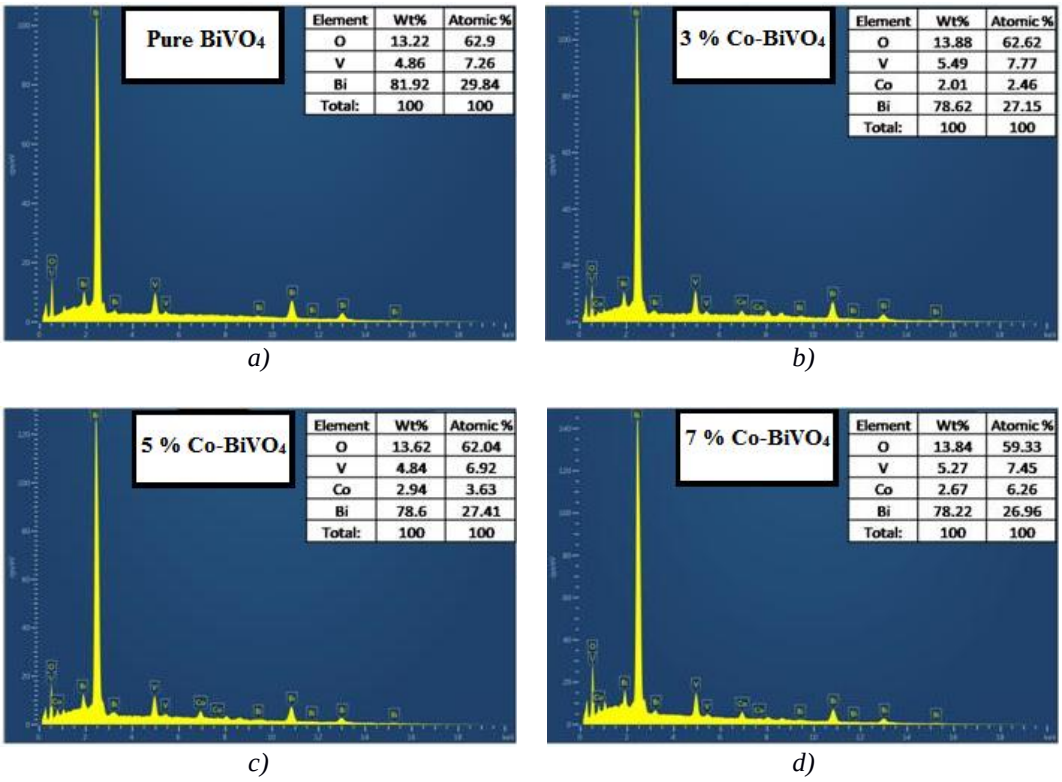

Fig. 3. EDAX spectra of synthesized a) Pure $BiVO_4$ b) 3% Co doped $BiVO_4$ c) 5% Co doped $BiVO_4$ & d) 7% Co doped $BiVO_4$ Nanoparticles.

3.4. UV-Vis Diffuse Reflectance Spectral and Band-gap Analysis

The diffuse reflectance spectra and optical band gap (Eg) region was studied by UV-Vis diffuse reflectance measurements in the UV-Vis region. The band gap in the semiconductor materials changes as the dopant creates the crystal imperfection. Fig. 4 (a) shows the diffuse reflectance spectra of pure and Co-doped $BiVO_4$ samples with various concentration and subsequent calcination at 450^{o}C for 2 h. In Fig. 4(a) it is noted that the reflectance spectra in the range of 200-1400 nm for all the investigated samples and it is found to decrease with increasing Co content. Also, the optical intensity of reflectance in the visible region varies, depending on the dopant concentrations. This systematic variation for the Co-doped samples compared with the pure $BiVO_4$ sample confirms the substitution of Co. In addition, the indirect band gap energies (Eg) were calculated according to the formula (4)

$$\alpha hv = A\,(hv - Eg)^{n/2} \tag{4}$$

where α, h, v, A and Eg stand for the absorption coefficient, Planck's constant, the frequency of light, a constant and the band gap energy respectively. The term n is determined by the characteristic optical transition of a metal oxide (n = 1 and n = 4 for a direct transition and an indirect transition). Fig. 4 (b) shows that the band gap energy of the studied samples was determined by plotting $[F(R)*hv]^2$ Vs. hν and extra polating the linear part of the curve $[F(R)*hv]^2$ to zero. The optical band gap obtained amounts to 2.842 eV, 2.696 eV, 2.594 eV and 2.538 eV respectively for x = 0%, 3%, 5% and 7% respectively. The band gap energies decreases with increasing the dopant concentration and their detected the red shift in the gap energy can be explained by the doping phenomenon. Yet, the analogue decrease in the band gap was also observed and it may be revealed that this shift asserts the uniform substitution of Co^{2+} ions in the $BiVO_4$ lattice. Besides, the effects of many bodies on the conduction and valence bands could be the cause of the reduction of the forbidden band which can reduce this band and result from the

electron interaction and diffusion of impurities. This has been assigned to the fusion of a band of impurities with a conduction band, which, in turn, led to the reduction of band gap.

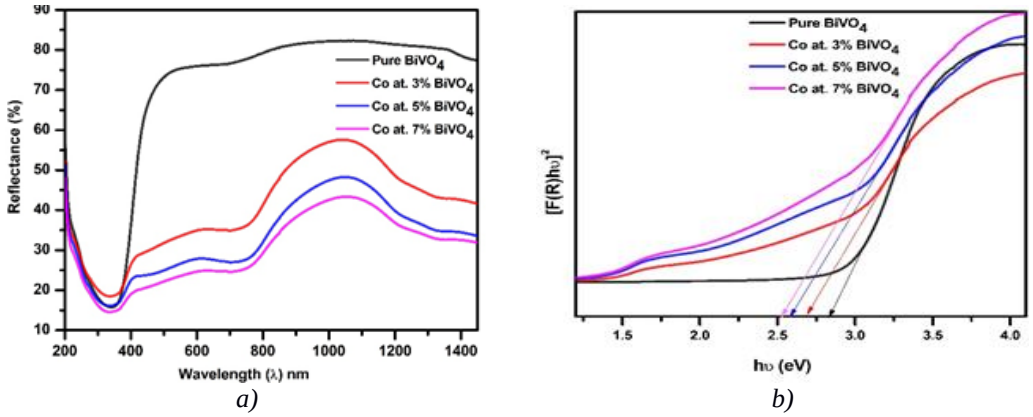

Fig. 4. (a) Diffuse reflection spectra, (b) Optical Band-gap plots of $BiVO_4$ and Co doped $BiVO_4$ NPs. The inset of (a) shows the hump related to transition of Co ion and inset of (b) shows red shift in the band gap of the $BiVO_4$ NPs with increase in Co content.

3.5. PL Spectra Analysis

The PL spectra of synthesized Pure $BiVO_4$ and various concentration of Co doped $BiVO_4$ nanoparticles were shown in Fig. 5. Photoluminescence spectra of prepared nanoparticles exhibit emission peak around 510 nm for Pure $BiVO_4$ and Co doped $BiVO_4$ (3%, 5% &7%) nanoparticles agreeing to emissions of ultraviolet due to NBE excitonic emission process. The peak at nearby 510 nm can be accredited to the recombination of some extrinsic radioactive transitions, such as charges recombination between the shallows level and intrinsic bands or recombination of donor-acceptor pairs. The weak green emission band was observed at 515 nm and its intensity is found to decrease as the dopant concentration increases which may be due to a decrease in oxygen vacancy concentration.

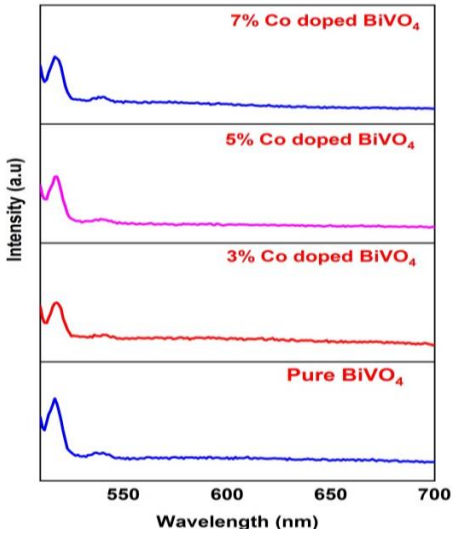

Fig. 5. PL spectra of synthesized a) Pure $BiVO_4$ b) 3% Co doped $BiVO_4$ c) 5% Co doped $BiVO_4$ & d) 7% Co doped $BiVO_4$ Nanoparticles.

4. Conclusions

Bismuth Vanadate nanoparticles were synthesized by co-precipitation method. The structural, morphological, elemental composition, absorption studies and optical analysis were carried out and the results were discussed in detail. The importance of nanotechnology as well as Bismuth Vanadate nanoparticles was discussed. XRD analysis reveals the orthorhombic structure and the average crystallite size are predicted to be in the range of 5.6-22 nm. SEM observations reveal the morphology of the prepared pure $BiVO_4$ and Co doped $BiVO_4$ nanoparticles were found to be clusters with tiny particles. EDAX analysis confirms the purity of prepared pure $BiVO_4$ and Co doped $BiVO_4$ nanoparticles. The band gap is red shifted as Co dopant into $BiVO_4$ system.

References

[1] Wei Tao, Na Kong, Xiaoyuan Ji, Yupeng Zhang, Amit Sharma, Jiang Ouyang, Baowen Qi, Junqing Wang, Ni Xie, Chulhun Kang, Han Zhang, Omid C. Farokhzad, Jong Seung Kim, Chem. Soc. Rev, **48**, 2891 (2019).

[2] Hyemin Kim, Songeun Beack, Seulgi Han, Myeonghwan Shin, Taehyung Lee Yoonsang, Park Ki, Su Kim Ali, K.Yetisen Seok, Hyun Yun, Woosung Kwon, Sei Kwang Hahn, Adv. Matter. **30**, 1 (2018).

[3] Bing Wang, Zhi Bin Zhang, Shi Peng Zhong, Zhao Qiang Zheng, Ping Xu, Han Zhang, J. Mater. Chem. C **8**, 4988 (2020).

[4] Zhao Wei, Dai Benlin, Zhu Fengxia, Tu Xinyue, Xu Jiming, Zhang Lili Li, Shiyin Dennis, Applied Catalysis B: Environmental **229,** 171 (2018).

[5] Chomkitichai Weerasak, Applied Mechanics and Materials **886**, 138 (2019).

[6] Lan Zhou, Aniketa Shinde, Santosh K. Suram, Helge S. Stein,Sage R. Bauers, Andriy Zakutayev, Joseph S. DuChene, Guiji Liu, Elizabeth A. Peterson, Jeffrey B. Neaton, John M. Gregoire, ACS Energy Lett. **3**(11), 2769 (2018).

[7] Yongliang Cheng, Jiangtao Chen, Xingbin Yan, Zongmin Zheng, Qunji Xueb, RSC Adv. **3**, 20606 (2013).

[8] A. Malathia, J. Madhavan Muthupandian, Ashokkumar Prabhakar, Arunachalam, Applied Catalysis A: General **555**, 47 (2018).

[9] Qingguo Meng, Haiqin Lv, Mingzhe Yuan, Zhen Chen, Zhihong Chen, Xin Wang, ACS Omega **2**(6), 2728 (2017).

[10] Mohamad Fakhrul, Ridhwan, Samsudina Suriati, Sufian Robabeh, Bashiri Norani, Muti Mohamed Raihan, Mahirah Ramlia, Journal of the Taiwan Institute of Chemical Engineers **81**, 305 (2017).

[11] F. Li, L. Zhang, X. Chen, Y. L. Liu, S. G. Xua, S. K. Cao S. K, Phys. Chem. **19**, 21862 (2017).

[12] M. Anandan, S. Dinesh, N. Krishnakumar, K. Balamurugan, Mater. Res. Express 3(11), 5009.

[13] Norouzzadeh Kh. Mabhouti, M. M. Golzan, R. Naderali, Optik **204**, 164227 (2020).

[14] V. Jeevanantham, K. Hemalatha, S. Satheeskumar, Journal of Ovonic Research **14**(4), 269.

[15] S. Satheeskumar, V. Jeevanantham, D. Tamilselvi, Journal of Ovonic Research **14**, 9 (2018).